ORIGINAL PAPER

The effect of swelling on vocal fold kinematics and dynamics

Jonathan J. Deng[1] · Byron D. Erath[2] · Matías Zañartu[3] · Sean D. Peterson[1]

Abstract

Swelling in the vocal folds is caused by the local accumulation of fluid, and has been implicated as a phase in the development of phonotraumatic vocal hyperfunction and related structural pathologies, such as vocal fold nodules. It has been posited that small degrees of swelling may be protective, but large amounts may lead to a vicious cycle wherein the engorged folds lead to conditions that promote further swelling, leading to pathologies. As a first effort to explore the mechanics of vocal fold swelling and its potential role in the etiology of voice disorders, this study employs a finite-element model with swelling confined to the superficial lamina propria, which changes the volume, mass, and stiffness of the cover layer. The impacts of swelling on a number of vocal fold kinematic and damage measures, including von Mises stress, internal viscous dissipation, and collision pressure, are presented. Swelling has small but consistent effects on voice outputs, including a reduction in fundamental frequency with increasing swelling (10 Hz at 30 % swelling). Average von Mises stress decreases slightly for small degrees of swelling but increases at large magnitudes, consistent with expectations for a vicious cycle. Both viscous dissipation and collision pressure consistently increase with the magnitude of swelling. This first effort at modeling the impact of swelling on vocal fold kinematics, kinetics, and damage measures highlights the complexity with which phonotrauma can influence performance metrics. Further identification and exploration of salient candidate measures of damage and refined studies coupling swelling with local phonotrauma are expected to shed further light on the etiological pathways of phonotraumatic vocal hyperfunction.

Keywords Swelling · Vocal folds · Finite-element modeling · Tissue damage

1 Introduction

Vocal hyperfunction (VH) is a condition defined by excessive laryngeal musculature activation during phonation (Oates and Winkworth 2008). Despite the widely

accepted definition of VH in clinical practice, its etiology is poorly understood (Hillman et al. 2020). Vocal hyperfunction is delineated into phonotraumatic (PVH) and non-phonotraumatic (NPVH) subclasses, with the former being a hyperfunctional response due to trauma-induced swelling and structural pathology development (Hillman et al. 2020). Whether an initial hyperfunctional response develops into persistent PVH depends on whether normal spontaneous recovery of vocal function occurs or if the initial hyperfunctional response results in compensatory adjustments that elicit a further hyperfunctional response. The latter 'vicious cycle' eventually results in development of phonotraumatic lesions and persistent PVH (Hillman et al. 2020).

During swelling, fluid accumulates in the tissues resulting in changes in vocal fold (VF) shape and local tissue properties (Yang et al. 2017a), which alters their biomechanics. In addition to the role of swelling in hyperfunctional voice disorder development, swelling could also play a role in the apparent benefits of vocal warm up exercises. Vocal warm up exercises are thought to prevent vocal fatigue, decrease

✉ Sean D. Peterson
peterson@uwaterloo.ca

Jonathan J. Deng
j8deng@uwaterloo.ca

Byron D. Erath
berath@clarkson.edu

Matías Zañartu
matias.zanartu@usm.cl

[1] Department of Mechanical and Mechatronics Engineering, University of Waterloo, Waterloo, ON N2L 3G1, Canada

[2] Department of Mechanical and Aerospace Engineering, Clarkson University, Potsdam, NY 13699, USA

[3] Department of Electronic Engineering, Universidad Técnica Federico Santa María, Valparaíso, Chile

phonatory effort, improve voice quality, and potentially prevent injury (Elliot et al. 1995; Milbrath and Solomon 2003; Vintturi et al. 2001). Since minor swelling is one effect of voice usage, it could be a factor in the hypothesized benefits of vocal warm up on injury and vocal fatigue.

Swelling and fluid transport in biological tissues, including the VFs, is governed by Starling's equation (Starling 1896; Gou and Pence 2016), which relates flow across the capillaries into the tissue interstitial space to driving hydrostatic and osmotic pressure gradients. Swelling is induced when flow into the interstitial region exceeds the normal drainage rate (Gou and Pence 2016), although the specific mechanism that causes this increased movement of fluid varies depending on the triggering issue (Mortimer and Levick 2004). In cases of inflammation (which could be caused by a variety of factors from tissue mechanical damage to infection), for example, increased capillary permeability and capillary pressure contribute to increased flow from the capillaries (Mortimer and Levick 2004). For VFs, this could be caused by phonation-induced trauma, as shown by Verdolini et al. (2003), who found shifts in biochemical markers associated with inflammation in VF secretions after vocal loading. Czerwonka et al. (2008) proposed vibration-induced increases in capillary pressure as a potential trigger of inflammation and edema.

To the best of our knowledge, VF swelling and its impact on VF kinematics and kinetics has not been previously considered from the modeling perspective. However, stress-induced fluid flux in the VFs, associated with systemic hydration, has been considered. Zhang et al. (2008) employed a biphasic model to explore the influence of internal fluid flux on the viscoelastic behaviors of the VFs. They found that the biphasic model qualitatively captured stress–relaxation behavior of the VFs seen in previous experiments (Zhang et al. 2008), thus demonstrating the importance of hydration on the dynamics of the VFs. Bhattacharya and Siegmund (2014) used a single phase (solid) VF model with viscoelastic parameters derived from biphasic theory to predict fluid motion within the VFs. They found that collision-free phonation tends to cause increasing hydration because simulated flow velocities predicted an influx of fluid. However, fluid influx was only predicted as a post-processing step and did not affect the VF motion; that is, no swelling occurred. Erath et al. (2017) developed a simplified one-dimensional model of viscous damping to investigate the impact of hydration on viscous dissipation and collision pressures. They found that collision pressure was influenced by both tissue elasticity and interstitial fluid viscosity with a specific combination of elasticity and fluid damping resulting in minimal collision pressure. Wu and Zhang (2017) used a one-way coupled poroelastic/biphasic model where the VF motion was imposed a priori to drive internal fluid motion (fluid motion did not affect the solid motion so no swelling occurred) coupled with fluid transport at the medial surface and lateral boundary. Using this model, they found that loud phonation conditions (large amplitude motions) could induce systemic dehydration. Recently, Wu and Zhang (2022) investigated the effect of hydration-induced stiffness changes, based on the dehydration predicted in (Wu and Zhang 2017), on the dynamics of a self-oscillating VF model interacting with a glottal flow. While dehydration influenced the stiffness in their model, no changes in volume were considered. They found that dehydration levels impacted VF dynamics, albeit for high levels of dehydration.

Whereas these prior studies have demonstrated that intra-VF fluid flux can influence VF dynamics, they have focused solely on fluid redistribution or identified the conditions that would promote swelling as a post-processing step, and thus did not consider the impact of swelling itself. Swelling, on the other hand, results in a change in the total fluid volume within the VFs, which can change both soft tissue properties and total volume (Gou and Pence 2016), thus influencing structural pathology development. To study swelling in other soft tissues, past works have proposed models to capture changes in material properties and shape associated with the fluid accumulation. Triphasic models, comprising a solid extracellular matrix phase, an interstitial fluid phase, and a chemical species phase, have been proposed to describe osmotically driven swelling in cartilage (Lai et al. 1991). Specifically, changes in the concentration of the chemical species alters osmotic pressure, which can drive fluid flow into the interstitia (Wilson et al. 2005). Triphasic models are computationally expensive, however, making it difficult to model complex problems with large geometries (Wilson et al. 2005). An alternative approach suitable for modeling soft tissue swelling was introduced by Tsai et al. (2004), Pence and Tsai (2005a), and Pence and Tsai (2005b). In this approach, a swelling field is prescribed as a parameter that modifies a hyperelastic constitutive equation to produce swelling-induced changes in tissue properties. This strategy has been used to study angioedema (Gou and Pence 2016), cervical swelling (Gou et al. 2020), as well as the combined effects of tissue swelling and remodeling (Topol et al. 2018).

While modeling the formation of structural pathologies (e.g., nodules and polyps) in PVH requires knowledge of the mechanics driving localized swelling, herein we consider generalized VF swelling and its impact on vocal performance and damage measures. We posit that small amounts of swelling could trigger a hyperfunctional response that can lead to a vicious cycle of PVH, wherein modified VF dynamics from initial swelling leads to further swelling, and ultimately persistent PVH. We also consider the potential role of VF swelling in vocal warm up as a mechanism to prevent injury. We restrict swelling to the lamina propria as swelling in this region is commonly observed in the initial stages of voice usage (Bastian et al. 1990).

The remainder of the paper is organized as follows: Sect. 2 discusses the model setup, study design, and swelling model implementation; further details on the derivation of the swelling model are given in Appendix A. Section 3 presents the simulation results. Section 4 discusses the significance of the results, analyzes why swelling leads to the observed results, and discusses study limitations. Finally, Sect. 5 summarizes salient findings from this work.

2 Methodology

Herein we consider a two-dimensional (2D) representation of the VFs, as shown in Fig. 1, discretized with the finite-element method (FEM), which has been shown to compare well with experimental silicone VF studies (Hadwin et al. 2019). The VF geometry is based upon the M5 model (Scherer et al. 2001) (note the VF thickness is 5 mm, which is shorter than the physical model shown in (Scherer et al. 2001)) and left-right symmetry is assumed, such that only one VF needs to be considered. The internal VF structure is divided into body, cover, and epithelium layers (Hirano 1974), each with distinct nominal Young's moduli given by E_{body}, E_{cover}, and E_{epi}, respectively. This subscript convention is used throughout the remainder of the manuscript. All layers share the same nominal density ρ_{vf}. The internal VF domain is denoted Ω with boundary $\partial\Omega$. The body and cover domains are denoted Ω_{body} and Ω_{cover}, respectively, such that $\Omega = \Omega_{\text{body}} \cup \Omega_{\text{cover}}$. The epithelium is treated as a membrane and thus has zero area (Deng and Peterson 2022).

A Cartesian coordinate system for the reference configuration, $X \in \mathcal{R}^2$, is defined with origin on the tracheal wall at the inferior margin of the VF as shown in Fig. 1. An additional
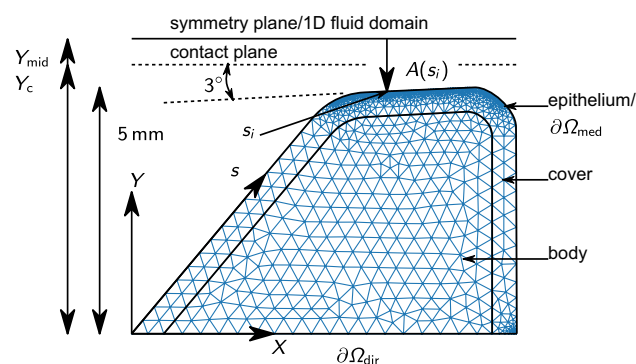

Fig. 1 Schematic of the vocal fold geometry in the reference configuration with representative finite-element discretization. Two finite thickness layers are indicated by 'body' and 'cover,' whereas the 'epithelium' layer is treated as a membrane (infinitesimally thin) along the surface $\partial\Omega_{\text{med}}$. Material coordinates $X = (X, Y)$ and s indicate 2D coordinates and medial surface/1D fluid domain coordinates, respectively; i denotes nodal indices along the medial surface. The glottal area is denoted by A (half the glottal area is shown due to symmetry)

surface coordinate, $s \in \mathcal{R}$, is defined along the VF boundary that is contact with the fluid, denoted as $\partial\Omega_{\text{med}}$ (note, this corresponds to the surface comprising the epithelium membrane). The fixed (Dirichlet) VF boundary region at the interface with the tracheal wall is denoted $\partial\Omega_{\text{dir}}$ such that $\partial\Omega = \partial\Omega_{\text{dir}} \cup \partial\Omega_{\text{med}}$.

Aerodynamic loading on the VF assumes the driving flow to be inviscid, incompressible, quasi-steady, and one-dimensional (1D) such that Bernoulli's equation can be computed along the centerline streamline then imposed upon the VF surface. The influence of acoustic loading on the VF dynamics is assumed negligible, i.e., only level 1 interactions (Titze 2008) are considered.

Models for the glottal flow and VFs were chosen as a balance of fidelity and computational simplicity, to make parametric studies feasible with available resources. A 2D model, while it will not capture 3D effects, has been shown to compare well with experimental silicone VF studies (Hadwin et al. 2019) and likely is applicable to situations with long VFs where the plane-strain assumption approximately applies. Similarly, 1D models of the glottal flow are computationally simple but compare qualitatively well with more complicated 2D Navier–Stokes-based models (Decker and Thomson 2007). These simplifications were considered reasonable since the focus of our study is to determine if general effects of swelling can trigger a vicious cycle, rather than to make accurate quantitative predictions.

2.1 Finite-element formulation

Let the reference configuration (Fig. 1) with coordinates X correspond to the unswollen, unstressed state of the VFs. While deformations of the VFs are normally small enough to justify the small-strain assumption, the constitutive model for swelling (described in detail in Appendix A) results in prestress for the material constitutive response in the reference configuration, which invalidates the small-strain assumption. As a result, we assume large deformations for the material strain energy (which includes the effect of swelling) and small deformations for remaining terms; the weak form of conservation of linear momentum for the solid domain Ω then follows from the principle of virtual work, see Bathe (2006, Chapter 4 and Chapter 6) for example. In the present case, this yields

$$\int_{\Omega} \rho(v)\ddot{u} \cdot \delta u + S(E, v) : \delta E + \eta\dot{\epsilon} : \delta\epsilon \, dX$$
$$+ \int_{\partial\Omega_{\text{med}}} \sigma_{\text{epi}} : \delta\epsilon_{\text{epi}} d_{\text{epi}} \, ds \qquad (1)$$
$$= \int_{\partial\Omega_{\text{med}}} t \cdot \delta u \, ds \text{ for all } \delta u \in \mathcal{V}^2(\Omega),$$

where $\mathcal{V}(\Omega)$ is the space of scalar piece-wise linear functions over a triangular mesh (shown in Fig. 1) equal to 0

on $\partial\Omega_{\text{dir}}$, $\boldsymbol{u}, \dot{\boldsymbol{u}}, \ddot{\boldsymbol{u}} \in \mathcal{V}^2(\Omega)$ are the displacement, velocity, and acceleration vectors, respectively, and $\delta\boldsymbol{u} \in \mathcal{V}^2(\Omega)$ is a virtual displacement. Strain tensors $\boldsymbol{E} = 1/2(\boldsymbol{F}^T\boldsymbol{F} - \boldsymbol{I})$ and $\boldsymbol{\epsilon} = 1/2(\boldsymbol{F} + \boldsymbol{F}^T) - \boldsymbol{I}$ are the Green strain and the small-strain tensor, respectively, where $\boldsymbol{F} = \partial\boldsymbol{u}/\partial\boldsymbol{X} + \boldsymbol{I}$ is the deformation gradient. Similarly, virtual strains are given by $\delta\boldsymbol{E} = 1/2(\delta\boldsymbol{F}^T\boldsymbol{F} + \boldsymbol{F}^T\delta\boldsymbol{F})$ and $\delta\boldsymbol{\epsilon} = 1/2(\delta\boldsymbol{F} + \delta\boldsymbol{F}^T)$, where $\delta\boldsymbol{F} = \partial\delta\boldsymbol{u}/\partial\boldsymbol{X}$ is the virtual deformation gradient. The corresponding stress tensors are the second Piola–Kirchhoff stress tensor, $\boldsymbol{S}$, and the Cauchy stress tensor, $\boldsymbol{\sigma}$.

The strain energy terms $\int_\Omega \boldsymbol{S}(\boldsymbol{E}, v) : \delta\boldsymbol{E} + \eta\dot{\boldsymbol{\epsilon}} : \delta\boldsymbol{\epsilon}\, d\boldsymbol{X}$ are based on an ad hoc modification of the Kelvin–Voigt model to account for swelling. The classical Kelvin–Voigt model gives the Cauchy stress as $\boldsymbol{\sigma} = \boldsymbol{K}\boldsymbol{\epsilon} + \eta\dot{\boldsymbol{\epsilon}}$ (Fung 1993; Zheng et al. 2010), where $\boldsymbol{K}\boldsymbol{\epsilon}$ is the elastic stress and $\boldsymbol{K}$ is the elasticity tensor, and $\eta\dot{\boldsymbol{\epsilon}}$ is the viscous stress and η is the viscosity. Using the approach developed in (Tsai et al. 2004; Pence and Tsai 2005a; Gou and Pence 2016), swelling is modeled for hyperelastic materials by modifying the hyperelastic constitutive equation. As a result, we replace the elastic stress in the Kelvin–Voigt model by a hyperelastic material stress with swelling effects while keeping the unmodified viscous term, resulting in

$$\boldsymbol{\sigma} = (\det\boldsymbol{F})^{-1}\boldsymbol{F}\boldsymbol{S}(\boldsymbol{E}, v)\boldsymbol{F}^\top + \eta\dot{\boldsymbol{\epsilon}},$$

where $\boldsymbol{S}(\boldsymbol{E}, v)$ is dependent on the swelling field, v, and Green strain, $\boldsymbol{E}$, through the swelling constitutive equation introduced in Sect. 2.2. Note $v = 1$ implies no swelling (no volume change), while $v = 1.2$ represents a 20 % increase in the free volume (volume with no external loading). In the virtual work statement, the viscous stress is a Cauchy stress work-conjugate with the virtual small strain, while the hyperelastic stress is a second Piola–Kirchhoff stress work-conjugate with the virtual Green strain (Gurtin et al. 2010).

The material density ρ in Eq. (1) requires special consideration in the case of swelling. Since swelling introduces additional mass into the system, ρ is given by

$$\rho = \rho_0 + (v - 1)\rho_v, \tag{2}$$

where ρ_0 is again the nominal density in the absence of swelling (that is, at $v = 1$) and ρ_v is the density of the incoming material causing the swelling, which is assumed to be water. Per unit volume in the reference configuration, the first term of Eq. (2) represents the original mass of material and the second term represents the additional mass due to the influx of fluid with swelling. Note that Eq. (2) considers density in the reference configuration; the density in the deformed configuration will be approximately ρ_0 as the VF volume will increase with swelling.

The first three terms in the first integral of Eq. (1) represent the virtual work due to inertial forces, material strain energy, and viscous effects. The second integral term in

Eq. (1) represents the strain energy contribution due to an epithelium over the medial surface, where $\boldsymbol{\sigma}_{\text{epi}}$ and $\boldsymbol{\epsilon}_{\text{epi}}$ are the membrane stress and strain tensors, respectively (Hansbo and Larson 2014; Deng and Peterson 2022). A separate epithelium was included because past studies found the epithelium to significantly influence VF dynamics (Murray and Thomson 2012; Xuan and Zhang 2014; Tse et al. 2015; Hadwin et al. 2021; Deng and Peterson 2022); furthermore, the epithelium herein acts as an outer barrier that constrains internal swelling, thus affecting the shape of the swollen material. The third term in Eq. (1) represents the surface traction on $\partial\Omega_{\text{med}}$ due to aerodynamic loading and VF collision. In this term, $\boldsymbol{t}$ represents the surface traction, which is discussed in further detail in Sect. 2.3.

2.2 Swelling-generalized constitutive equation

Following the approach laid out in Tsai et al. (2004), Pence and Tsai (2005a), Gou and Pence (2016), the constitutive equation employed herein is based on a generalized form for a hyperelastic material. Briefly, the generalized form for swelling of a hyperelastic material with strain energy function $\psi(\boldsymbol{F})$ is given by $\bar{\psi}(\boldsymbol{F}, v) = m(v)\psi(v^{-1/3}\boldsymbol{F})$, where $\bar{\psi}$ is the swelling-generalized strain energy, and m is a monotonic scalar function satisfying $m(1) = 1$ (Tsai et al. 2004, Equation 3). In the modified strain energy, $\bar{m}(v) = m/v$ controls the change in stiffness of the swollen material (see Appendix A), where its slope governs whether the material stiffness increases or decreases with swelling; if, for example, $\bar{m}' = d\bar{m}/dv < 0$, modulus softening of the swollen material occurs (Pence and Tsai 2005a; Gou et al. 2020). For a Saint Venant–Kirchhoff material, this results in

$$\boldsymbol{S} = \left(\bar{m}'(v - 1) + 1\right)v^{1/3}$$
$$\left(\frac{Ev}{(1+v)(1-2v)}(\text{Tr}\,\bar{\boldsymbol{E}})\boldsymbol{I} + \frac{E}{1+v}\bar{\boldsymbol{E}}\right), \tag{3}$$
$$\bar{\boldsymbol{E}} = \frac{1}{2}(\bar{\boldsymbol{F}}^\top\bar{\boldsymbol{F}} - \boldsymbol{I}) = v^{-2/3}\boldsymbol{E} + \frac{1}{2}(v^{-2/3} - 1)\boldsymbol{I},$$

where E and v are Young's modulus and Poisson's ratio, respectively. The term $\left(\bar{m}'(v - 1) + 1\right)$ represents the linearized effect of $\bar{m}(v)$ about $v = 1$. The swelling-modified Green strain tensor, $\bar{\boldsymbol{E}}$, contains an additional strain term $1/2(v^{-2/3} - 1)\boldsymbol{I}$ that creates a hydrostatic pressure that results in the swelling (see Appendix A).

2.3 Fluid and contact models

The surface traction $\boldsymbol{t}$ results from fluid pressures based on the Bernoulli equation and contact (Deng and Peterson 2022). Contact was modeled by a penalty method (Wriggers 2006) and the collision pressure is given by

$$p_c = k_c \left(\frac{\max\{g(X), 0\}}{2} \right)^3, \tag{4}$$

$$g(X) = Y - Y_c, \tag{5}$$

where k_c is the contact spring stiffness and g is the contact gap. Note that the term $\max\{g(X), 0\}$ ensures that the contact gap is positive when the VFs are contacting and 0 otherwise. A cubic contact spring is employed to ensure continuity of first and second derivatives of p_c at contact.

The Bernoulli equation is given by

$$p(s_i) = \begin{cases} p_{\text{sub}} + \frac{\rho_{\text{air}}}{2} q^2 \left(\frac{1}{A_{\text{sub}}^2} - \frac{1}{A(s_i)^2} \right) & s < s_{\text{sep}} \\ p_{\text{sep}} & s \geq s_{\text{sep}} \end{cases}$$

$$q^2 = \frac{2}{\rho_{\text{air}}} \left(\frac{1}{A_{\text{sep}}^2} - \frac{1}{A_{\text{sub}}^2} \right)^{-1} (p_{\text{sub}} - p_{\text{sep}})$$

$$A_{\text{sep}} = r_{\text{sep}} A_{\text{min}}$$

$$A_{\text{min}} = \min_{s_i} A(s_i)$$

$$A(s_i) = \max\{2(y_i - Y_c), A_{\text{lb}}\}, \tag{6}$$

where p is pressure, q is flow rate, ρ_{air} is the air density, r_{sep} is the separation area ratio, and A is the cross-sectional area of the glottis (see Fig. 1). Subscripts 'sep' and 'sub' denote quantities at the separation point and subglottal region, respectively. Areas A_{min} and A_{lb} represent the minimum glottal area and a lower bound on the glottal area function. Specifically, A_{lb} is used to define a 'safe' area (Anderson et al. 2013), which is employed in practice to prevent negative areas that can occur from the penalty contact method. As a result, instead of $A(s)$ in Eq. (6), the safe area

$$A_{\text{safe}}(s) = \begin{cases} A(s) & A(s) > A_{\text{lb}} \\ A_{\text{lb}} & A(s) \leq A_{\text{lb}} \end{cases}, \tag{7}$$

is used.

The final surface traction term is then due to both contact and fluid pressures and is given by

$$t = -p \det \boldsymbol{F} \boldsymbol{F}^{-\top} \boldsymbol{n} - p_c \boldsymbol{n}_c, \tag{8}$$

where $\boldsymbol{n}_c$ is the contact normal. Due to left-right symmetry of the VFs, the contact normal is constant and given by $\boldsymbol{n}_c = (0, 1)$.

2.4 Numerical solution

To integrate Eq. (1) in time, we used the Newmark-beta method (Newmark 1962) to approximate $\dot{\boldsymbol{u}}, \ddot{\boldsymbol{u}}$ at time step $n + 1$ using

$$\dot{\boldsymbol{u}}^{n+1} = \frac{\gamma}{\beta \Delta t}(\boldsymbol{u}^{n+1} - \boldsymbol{u}^n) - \left(\frac{\gamma}{\beta} - 1 \right) \dot{\boldsymbol{u}}^n - \Delta t \ddot{\boldsymbol{u}}^n \left(\frac{\gamma}{2\beta} - 1 \right) \tag{9}$$

$$\ddot{\boldsymbol{u}}^{n+1} = \frac{1}{\beta \Delta t^2}(\boldsymbol{u}^{n+1} - \boldsymbol{u}^n - \Delta t \dot{\boldsymbol{u}}^n) - \left(\frac{1}{2\beta} - 1 \right) \ddot{\boldsymbol{u}}^n \tag{10}$$

where superscripts n denote time indices (for example, $\ddot{\boldsymbol{u}}^n = \ddot{\boldsymbol{u}}(X, t^n)$), $\gamma = 1/2$ and $\beta = 1/4$ were chosen for stability, and $\Delta t = 1.25 \times 10^{-5}$ s. The choice of Δt and mesh size were based on an independence study described in Appendix B. Substituting Eqs. (9) and (10) into Eq. (1) yields a set of recursive relations for the state $\boldsymbol{u}^{n+1}, \dot{\boldsymbol{u}}^{n+1}, \ddot{\boldsymbol{u}}^{n+1}$ from known conditions at n. The initial state $n = 0$ is set as the static equilibrium state from Eq. (1) without external loads (no Bernoulli pressure) but with swelling. External loads are applied for all remaining time steps. The system of equations was solved using the FEniCS library (Logg and Wells 2010; Logg et al. 2012).

A parametric study over varying swelling values $v = 1.0, 1.05, \ldots, 1.25, 1.3$ and $\bar{m}' = 0.0, -0.4, -0.8, -1.2, -1.6$ was performed. The range of swelling parameter, v, was chosen based on an extreme level of systemic dehydration for children of 10 % (Friedman et al. 2004; King et al. 2018); since local hydration changes are likely larger than systemic levels, a maximum swelling level of 30 % was employed. Swelling was restricted to the cover layer based upon clinical observations which found fluid retention primarily occurred in the superficial lamina propria (Bastian et al. 1990). Swelling-induced stiffness change, $\bar{m}'$, was chosen based on the study by Yang et al. (2017b) where they measured force–displacement curves as a function of dehydration. Equation (3) implies a 1D modulus for a uniaxial stress test of $k(v) = (\bar{m}'(v - 1) + 1)E$ so that $k(v)/k(1) = \bar{m}'(v - 1) + 1$, where $k(v)$ denotes the 1D modulus for swelling level v. Rearranging yields

$$\bar{m}' \approx \left(\frac{k(v)}{k(1)} - 1 \right)(v - 1)^{-1}. \tag{11}$$

Using 1D modulus values from Yang et al. (2017b, Tables 2 and 3), we computed $\bar{m}'$ according to different values of $k(v)$ formed from the average of reported loading/unloading modulus values. Dehydration levels were converted to swelling levels assuming an initial water content by volume of 80 %. Over the varying dehydration/swelling levels, we found swelling-induced stiffness change varied from $\bar{m}' \approx -0.4$ to -1.6 (with more negative values at higher dehydration), so values from 0.0 to -1.6 centered around a nominal value of -0.8 were chosen.

All remaining model parameters were fixed and chosen based on past studies and experimental values, as summarized in Table 1. Elastic moduli were chosen based on values used in Alipour-Haghighi et al. (2000), Chhetri et al. (2011),

Table 1 Summary of fixed model parameter values

Parameter	Value
ρ_0, ρ_v	$1 \, \text{g/cm}^3$
E_{cover}	2.5 kPa
E_{body}	5.0 kPa
E_{epi}	50 kPa
ν, ν_{epi}	0.4
η	5 P
d_{epi}	50 µm
Y_{mid}	0.53 cm (see Fig. 1)
Y_c	0.525 cm (see Fig. 1)
k_c	$1 \times 10^{15} \, \text{Pa/cm}^3$
p_{sub}	300 Pa
p_{sep}	0 Pa
r_{sep}	1.2
ρ_{air}	$1.2 \times 10^{-3} \, \text{g/cm}^3$
A_{lb}	$2(Y_{\text{mid}} - Y_c)$

Miri (2014) and Poisson's ratio ν was chosen to model near incompressibility while avoiding numerical instability due to volumetric locking (Bathe 2006, Section 4.4.3). Epithelium properties were chosen based on previous experimental studies (Hirano and Kakita 1985; Tse et al. 2015). The contact spring value was chosen to balance minimizing the contact overlap while preventing ill-conditioning of the stiffness matrix (Wriggers 2006). Subglottal and separation pressures were chosen based on physiological ranges during speech (Zhang 2016), and $r_{\text{sep}} = 1.2$ was chosen based on usage in past studies (Decker and Thomson 2007; Hadwin et al. 2021).

3 Results

In this section, we present results for static parameters (volume and VF geometry changes induced by swelling), acoustic and kinematic outputs (fundamental frequency, SPL, and glottal width amplitude), and measures of VF damage (von Mises stress, viscous dissipation rate, and collision pressure) for varying levels of swelling and swelling-induced stiffness change. We also present results showing the impact of separate swelling-induced effects, specifically, swelling-induced mass, stiffness, and prephonatory gap changes, on the measures of VF damage.

3.1 Static parameters

We first consider the influence of swelling on the shape and mass of the VF without external fluid loading (expansion under swelling only). Generalized swelling throughout the cover was considered to represent phonotraumatic damage

distributed throughout the cover after normal voice usage as seen in experimental studies (Bastian et al. 1990). Figure 2 compares the nominal VF geometry with that of a VF with 30% swelling in the cover layer ($v = 1.30$) and swelling-induced relaxation ($\bar{m}' = -0.8$). Swelling leads to an outwards expansion of the medial surface due to the increase in volume of the cover layer. The remainder of the cover layer also experiences swelling, though to a lesser degree due to the fixed constraint at the intersection with $\partial \Omega_{\text{dir}}$. The body layer remains nearly fixed when swelling occurs except for a slight expansion adjacent to the medial surface that arises because of the expansion of the cover.

The increase in VF volume with swelling is shown quantitatively in Fig. 3. The actual volume increase is smaller than the prescribed swelling (close to 20 % for 30 % swelling) due to the action of external forces on the cover layer and the slight compressibility of the cover. The corresponding mass increase is linearly related to the prescribed swelling based on the linear relationship given in Eq. (2).
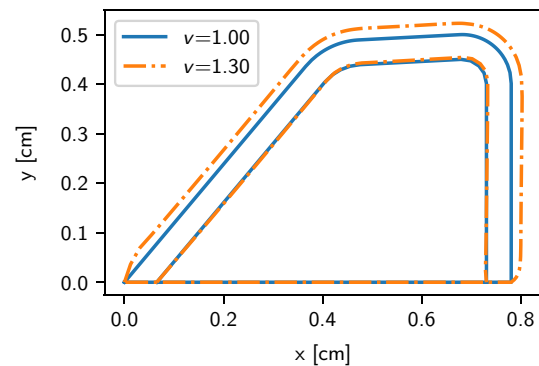
Fig. 2 Vocal fold geometry for the swollen ($v = 1.3$, dash-dotted lines) and original ($v = 1.0$, solid lines) states for intermediate swelling-induced softening ($\bar{m}' = -0.8$). Displacements due to swelling are exaggerated by two times for clarity
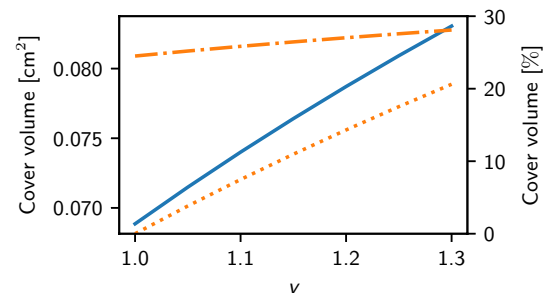
Fig. 3 Vocal fold cover volume as a function of swelling level, v, for intermediate swelling-induced softening ($\bar{m}' = -0.8$). The left abscissa shows the absolute cover volume (solid line). The right abscissa shows the change in cover volume relative to the initial cover volume (dotted line) and the cover volume relative to the total vocal fold volume (dash-dotted line)

3.2 Acoustic and kinematic outputs

Figure 4 presents the effect of swelling on kinematic and acoustic outputs. To compute the effect of swelling on fundamental frequency (f_o), we detect peaks of the glottal width waveform ($A_{min}(t)$) and measure the average period between peaks. To compute SPL, we use the flow rate [$q(t)$ from Eq. (6)] and the piston-in-baffle approximation (Kinsler et al. 2000, Section 7.4) at 1 m; this model gives the radiated pressure from an idealized piston sound source. The drop in frequency is about 10 Hz while the reduction in SPL is about 0.5 dB over the range $v = 1.0$ to 1.3. A small increase in SPL is present for small amounts of swelling despite consistently decreasing amplitudes of motion (Fig. 4) likely due to slight changes in the frequency content of harmonics. Both SPL and f_o also vary with swelling-induced stiffness change ($\bar{m}'$). Greater swelling-induced softening corresponds to larger f_o and SPL decreases for the same level of swelling.

3.3 Vocal fold damage measures

We consider three candidate metrics to assess potential VF damage (phonotrauma), namely von Mises stress, viscous dissipation, and collision pressure, defined as follows. The von Mises stress is given by $\sigma_{vm} = \sqrt{3/2\sigma_{dev} : \sigma_{dev}}$, where $\sigma_{dev} = \sigma - 1/3(\text{Tr}\,\sigma)I$ is the deviatoric part of the Cauchy stress. Spatial fields of viscous dissipation are defined by
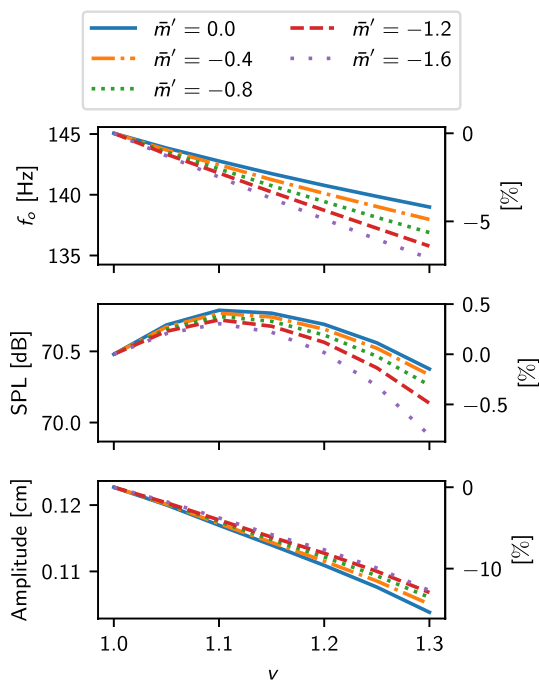
Fig. 4 Fundamental frequency (f_o), SPL at 1 m, and glottal width waveform amplitude as a function of swelling level (v) and swelling-induced stiffness change ($\bar{m}'$). The right abscissa shows the percent change from the initial value

$w_{visc} = \eta\dot{\epsilon} : \dot{\epsilon}$ and spatial fields of collision pressure, p_c, are given in Eq. (4).

To quantitatively compare these spatially and temporally varying variables, we compute the spatial and temporal averages as follows. For a function $f(X, t)$ (representing von Mises stress or viscous dissipation), the spatiotemporal average and temporal average, denoted by $\hat{f}$ and $\tilde{f}$, respectively, are defined as

$$\hat{f} = \underset{X,t}{\text{avg}}\, f(X, t) = \frac{\int_{0.25}^{0.5} \int_{\Omega_{cover}} f(X, t)\, dX dt}{\int_{0.25}^{0.5} \int_{\Omega_{cover}} dX dt}, \quad (12)$$

$$\tilde{f} = \underset{t}{\text{avg}}\, f(X, t) = \frac{\int_{0.25}^{0.5} f(X, t)\, dt}{\int_{0.25}^{0.5} dt}, \quad (13)$$

where the time integration limits of (0.25, 0.5) represent the last half of the time series.

In the case of contact quantities, we compute similar averages but only count instances where contact occurs. These averages are given by

$$\hat{f} = \underset{s,t}{\text{avg}}\, f(s, t) = \frac{\int_{0.25}^{0.5} \int_{\partial\Omega_{med}} H(g(s, t))f(s, t)\, ds dt}{\int_{0.25}^{0.5} \int_{\partial\Omega_{med}} H(g(s, t))\, ds dt}, \quad (14)$$

$$\tilde{f} = \underset{t}{\text{avg}}\, f(s, t) = \frac{\int_{0.25}^{0.5} H(g(s, t))f(s, t)\, dt}{\int_{0.25}^{0.5} H(g(s, t))\, dt}, \quad (15)$$

where H is the Heaviside step function and $g(s, t)$ is the contact gap from Eq. (4); note $H(g(s, t))$ is 1 when contact occurs and is 0 otherwise.

Figure 5 shows time-averaged von Mises stress fields ($\tilde{\sigma}_{vm}$) for the no-swelling condition (first column) and as differences relative to the no-swelling condition as swelling increases (subsequent columns). In the inferior portion of the cover layer, increasing swelling causes a slight decrease in the von Mises stress (for example, $v = 1.10, \bar{m}' = -0.8$) although this decrease is less severe at higher swelling levels. In the medial and superior portions of the cover layer, increasing swelling consistently increases the von Mises stress. Within the body, increasing swelling causes minimal changes. Greater swelling-induced softening (negative $\bar{m}'$) tends to mitigate increases in von Mises stress at higher levels of swelling (see, for example, $v = 1.30$ for the different $\bar{m}'$ values).

Figure 6 summarizes the spatiotemporally averaged trends of von Mises stress ($\hat{\sigma}_{vm}$). Mean von Mises stress initially drops with increase in swelling (v) due to the decrease in von Mises stress in the inferior part of the cover. This is followed by a more substantial rise with further increases in swelling due to the effects of increasing
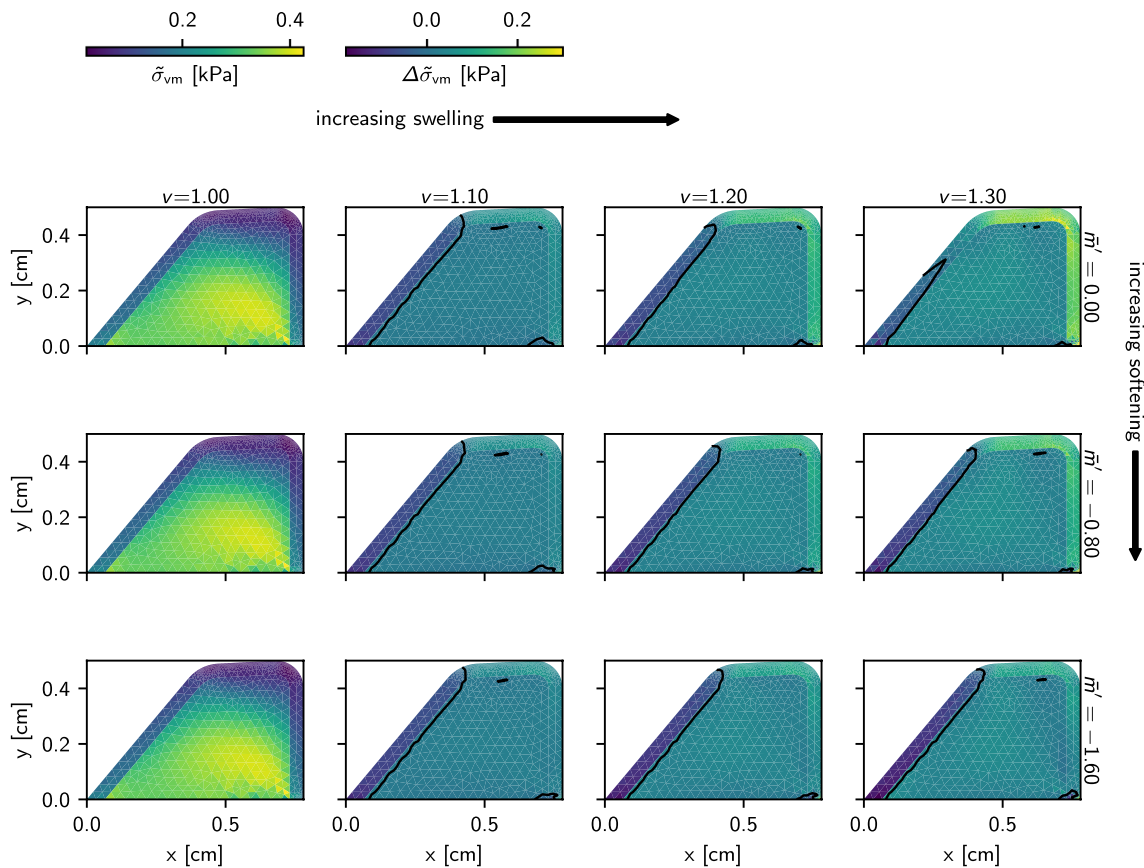
Fig. 5 Time-averaged (over the last 0.25 s) von Mises stress fields ($\tilde{\sigma}_{vm}$) as a function of swelling level (v) and swelling-induced stiffness change ($\bar{m}'$). The first column shows the absolute von Mises stress while the remaining columns show changes in von Mises stress relative to the no-swelling condition (first column $v = 1$). Regions with $\Delta\tilde{\sigma}_{vm} = 0$ are indicated by a solid dark contour for clarity
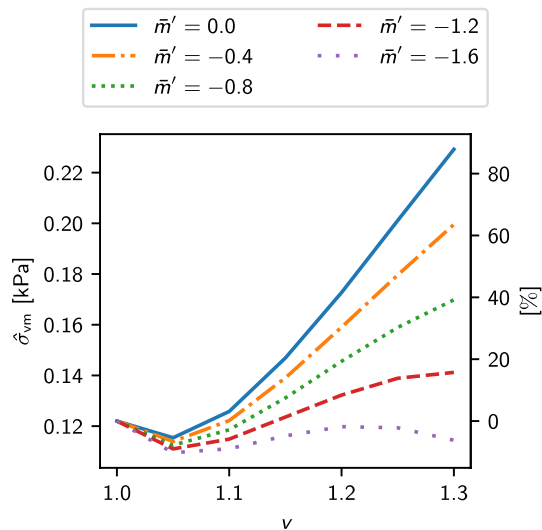

Fig. 6 Spatiotemporally averaged von Mises stress in the cover ($\hat{\sigma}_{vm}$) as a function of swelling level (v) and swelling-induced stiffness change ($\bar{m}'$). The right abscissa shows the percent change from the initial value

von Mises stress in the superior and medial parts of the cover. As seen in Fig. 5, greater swelling-induced softening tends to mitigate the rise in von Mises stress induced by swelling; for the greatest swelling-induced softening ($\bar{m}' = -1.6$), this effect is strong enough to slightly decrease von Mises stress for all swelling conditions.

Figure 7 presents time-averaged viscous dissipation fields ($\tilde{w}_{visc}$) for the no-swelling condition (first column) and as differences compared to the no-swelling condition (subsequent columns). Greater degrees of swelling increases viscous dissipation in the cover, which tends to be concentrated within the medial region of the cover where contact occurs. Greater swelling-induced softening (negative $\bar{m}'$) also results in increased viscous dissipation for the same level of swelling.

Analogous to Figs. 6, 8 shows the spatiotemporally averaged viscous dissipation rate in the cover ($\hat{w}_{visc}$). Clearly, viscous dissipation is affected by both swelling magnitude (v) and swelling-induced stiffness change ($\bar{m}'$). Greater swelling and/or swelling-induced softening both result in increased viscous dissipation.
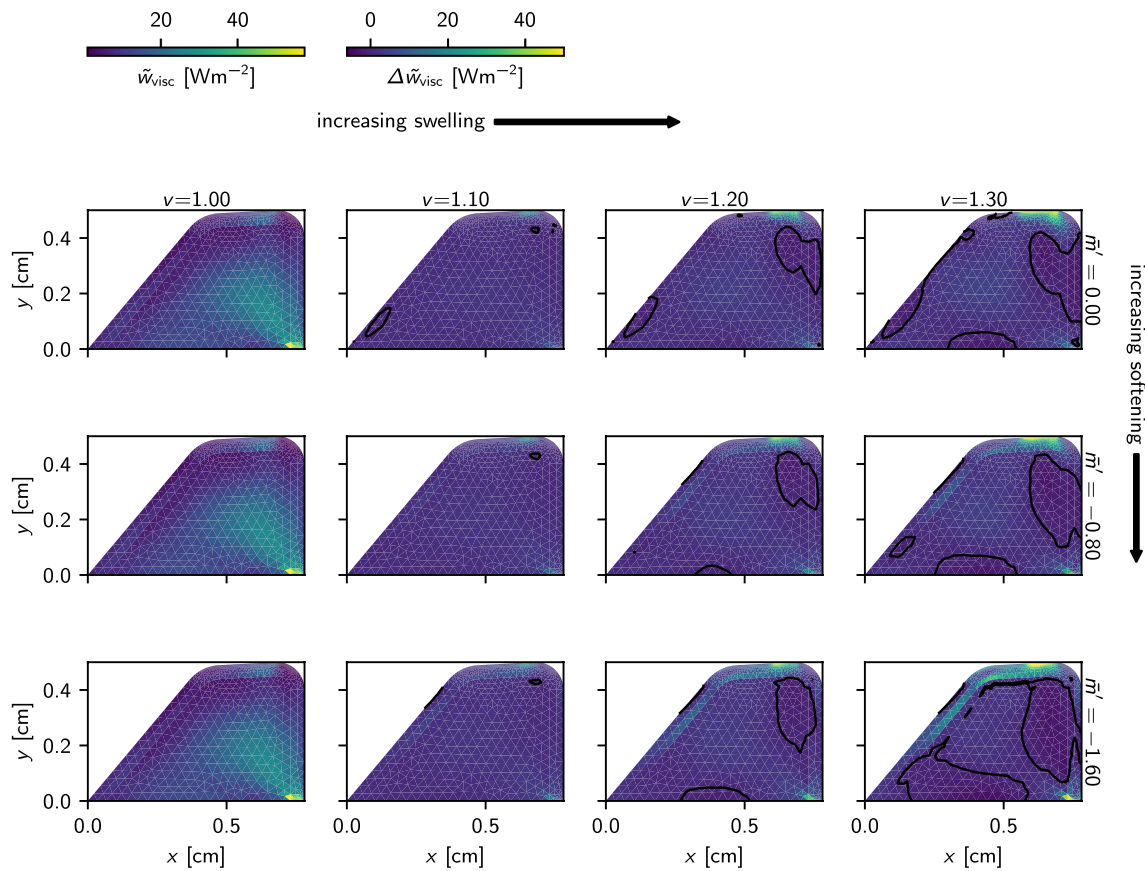
Fig. 7 Time-averaged viscous dissipation rate fields ($\tilde{w}_{\text{visc}}$) as a function of swelling level (v) and swelling-induced stiffness change ($\bar{m}'$). The first column shows absolute values of viscous dissipation rate; subsequent columns to the right show changes relative to the first column. Solid line contours indicate zero viscous dissipation change for clarity
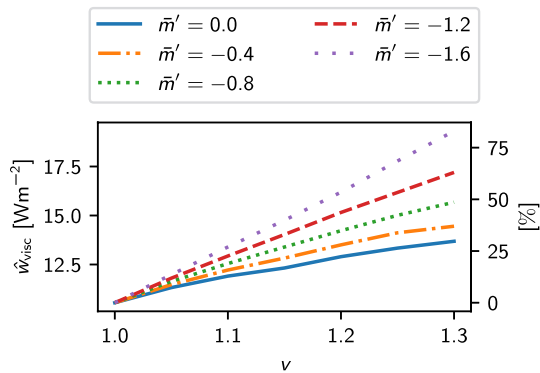

Fig. 8 Spatiotemporally averaged viscous dissipation rate in the cover ($\hat{w}_{\text{visc}}$) as a function of swelling level (v) and swelling-induced stiffness change ($\bar{m}'$). The right abscissa shows the percent change from the initial value

Figure 9 shows the time averaged collision pressure during VF collision ($\tilde{p}_c$). As swelling increases, so does collision pressure and contact area. Greater swelling-induced softening (negative $\bar{m}'$) reduces the magnitude of collision pressure and slightly reduces the contact area.

Figure 10 illustrates the temporal and spatial statistics of contact quantities over the contacting duration and areas. For the spatiotemporally averaged collision pressure ($\hat{p}_c$), Fig. 10 shows that increasing swelling (v) generally increases collision pressure (both average and maximum), except for a small dip in spatiotemporally averaged contact pressure for slight swelling ($v = 1.1$), which is exacerbated with increase in swelling-induced softening ($\bar{m}'$). In general, greater swelling-induced softening ($\bar{m}'$) reduces the increase in collision pressure with swelling. Contact area ($\tilde{A}_c$) is similarly affected with more swelling, leading to larger contact areas. Swelling-induced stiffness change has a small mediating effect where greater softening results in a slightly smaller contact areas.

3.4 Isolating the impact of swelling-induced effects on damage measures

In this section, we aim to isolate the influence of various swelling-induced effects on VF damage measures. Specifically, we decompose swelling into four constituent effects; namely, swelling-induced changes in:
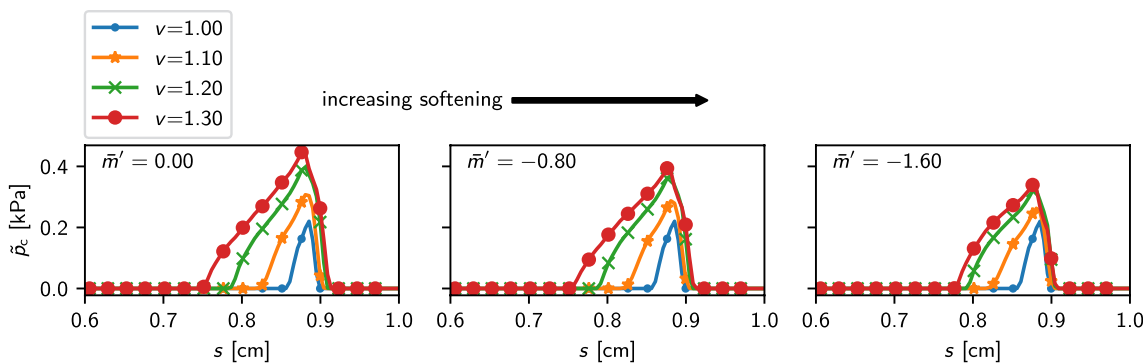
Fig. 9 Time-averaged (over the contacting duration) collision pressure distributions ($\tilde{p}_c$) as a function of swelling level (v) and swelling-induced stiffness change ($\bar{m}'$)

1. mass, arising from Eq. (2),
2. stiffness, arising from the term $\big(\bar{m}'(v-1)+1\big)$ in Eq. (3)
3. VF geometry from the hydrostatic pressure generated by the swelling-modified Green strain ($\bar{E}$) in Eq. (3), and
4. prephonatory gap (the minimum distance between the symmetry plane and VF surface in Fig. 1); the gap

change is related to the static deformation from swelling and a fixed symmetry plane.

To explore the isolated effects of swelling-induced changes in mass, stiffness, and prephonatory gap, we conducted simulations wherein the chosen parameters was held constant. For mass, this was accomplished by leaving the density constant; for stiffness this coincides with setting $\bar{m}' = 0$; for the gap change this involves shifting the symmetry plane (Y_{mid} in Table 1) to ensure the prephonatory gap remains fixed. To examine the effect of VF geometry change, we removed the other effects (mass, stiffness, and prephonatory gap change) and observed how the damage quantity changed with increase in swelling (which induced a VF geometry change). This was made possible because when these three effects are removed, only the swelling-induced VF geometry change effect remains. By then comparing against results with all influences included, the impact of the selected component could be assessed.
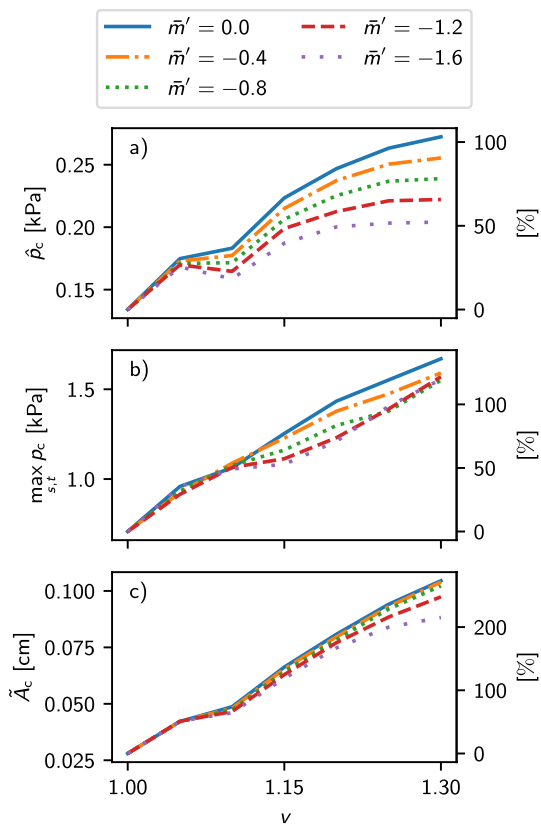
Figure 11 shows that each damage measure is affected by different swelling-induced changes. Spatiotemporally averaged von Mises stress ($\hat{\sigma}_{vm}$) is primarily affected by swelling-induced VF geometry changes and stiffness changes ($\bar{m}'$), as seen in Fig. 11 since the 'no stiffness change' trend differs significantly from the 'all swelling effects' trend. When only the VF geometry change effect is present ('no stiffness, mass, or gap change') von Mises stress increases with swelling (v), thus showing the effect of swelling-induced VF geometry change on von Mises stress. Swelling-induced mass, stiffness, and prephonatory gap all tend to increase spatiotemporally averaged viscous dissipation ($\hat{w}_{visc}$). Removing these three effects ('no stiffness, mass, or gap change') results in little variation of viscous dissipation with swelling, indicating that swelling-induced VF geometry changes have little impact. Swelling-induced softening (the 'no stiffness change' trend is above the 'all swelling effects' trend) tends to decrease spatiotemporally averaged collision pressure ($\hat{p}_c$), whereas swelling-induced mass and

Fig. 10 Statistics of contact quantities over the contacting duration and area consisting of a) spatiotemporally averaged collision pressure ($\hat{p}_c$), b) maximum collision pressure, and c) time-averaged contact area ($\tilde{A}_c$) as a function of swelling level (v) and swelling-induced stiffness change ($\bar{m}'$). In each case, the right abscissa shows the percent change from the initial value
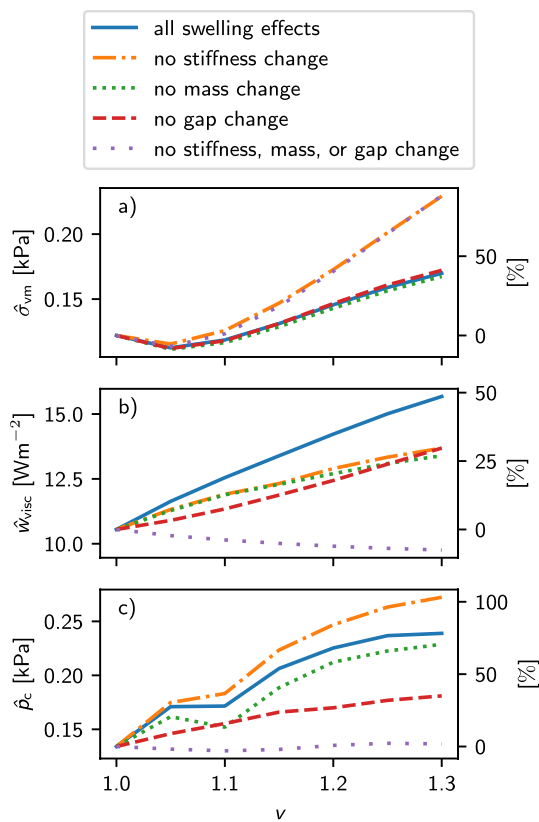
Fig. 11 Comparison of spatiotemporally averaged **a** von Mises stress ($\hat{\sigma}_{vm}$), **b** viscous dissipation ($\hat{w}_{visc}$), and **c** collision pressure ($\hat{p}_c$) trends versus swelling (v) with different swelling-induced effects removed and/or present for the intermediate swelling-induced softening ($\bar{m}' = -0.8$). In the case 'no stiffness, mass, or gap change', only swelling-induced geometry change remains. The right abscissa shows the percent change from the initial value

gap changes tend to increase collision pressure (the 'no mass change' and 'no gap change' trends are below the 'all swelling effects' trends). When these three effects are removed collision pressures vary only slightly with swelling, again indicating that swelling-induced VF geometry change has little effect.

4 Discussion

As expected, swelling clearly alters the shape and mass of the VFs. Mass change follows the linear relationship prescribed in Eq. (2). For the volume change, the medial surface predictably bulges outwards (Fig. 2); furthermore, because the body layer does not swell, the expansion of the cover layer also slightly expands the body by pulling it outwards. The slight expansion of the body layer is a result of the small but nonzero compressibility of the system.

As seen in Fig. 4, fundamental frequency (f_o) decreases with increase in swelling (v) and swelling-induced softening

($\bar{m}'$). Considering a spring–mass–damper analogy for the VF, swelling increases mass and decreases stiffness, both of which reduce frequency. Swelling-induced softening results in a larger stiffness reduction for the same degree of swelling, leading to a drop in fundamental frequency. Swelling has a small effect on SPL, where increasing swelling and/or swelling-induced softening tends to reduce SPL. We hypothesize this is due in part to the reduced prephonatory gap with swelling due to the bulging cover. Reduced prephonatory gap is associated with diminished vibration amplitudes (Fig. 4), leading to smaller flow rate waveform amplitudes and thus SPL. The changes in SPL were on the order of 0.5 dB, however, which is likely insignificant considering variations in SPL for a speaker between utterances have been measured at over 1 dB (Holmberg et al. 1994). The observed changes in SPL and f_o herein are qualitatively similar to changes in these quantities found in a recent study exploring the effect of dehydration-induced stiffness changes (Wu and Zhang 2022) (the reverse of swelling-induced softening studied herein) of 8.6 Hz and −0.4 dB, respectively, at 10 % systemic dehydration.

4.1 Damage measures

Swelling has differing effects on the various damage measures explored herein, with some showing propitious effects of swelling and others exhibiting detrimental trends, depending on the degree of swelling. As swelling increases, von Mises stress in the cover ($\tilde{\sigma}_{vm}$) is affected differently depending on the region. In the medial and superior parts of the cover, increased swelling consistently increased von Mises stress (Fig. 5), while in the inferior portion of the cover it experienced a slight decrease. The spatiotemporal average of von Mises stress over the cover ($\hat{\sigma}_{vm}$ shown in Fig. 6) exhibits a slight decrease with low degrees of swelling followed by a rapid rise as swelling increases further. Similarly, average contact pressure ($\hat{p}_c$ seen in Fig. 10a), though increasing initially with swelling, exhibits a plateau over a range of modest swelling. That is modest swelling may be beneficial, at least in terms of these particular damage measures, which is aligned with the clinical impression of the protective benefits of vocal warm up exercises in mitigating vocal fatigue and potentially vocal injury (Milbrath and Solomon 2003). In contrast, spatiotemporally averaged viscous dissipation ($\hat{w}_{visc}$) and maximum collision pressure (Figs. 8 and 10b, respectively) both exhibited detrimental effects with swelling.

The selected damage measures are primarily affected by different aspects of swelling (see Fig. 11) likely due to differing physical mechanisms that drive them. The von Mises stress, for example, is primarily affected by VF geometry changes and swelling-induced stiffness change (Fig. 11) likely due to the mechanism of cover deformation induced by

swelling (*v*). This is supported by differences in the von Mises stress distribution between the inferior part of the cover and the remainder. In the inferior portion of the cover, swelling acts to expand the cover while air pressure in the glottis tends to compress it, thus leading to less distortion and lower von Mises stress. Over the medial and superior surfaces, however, fluid pressures are negligible due to flow separation so the swelling-induced VF geometry change leads to distortions that purely increase von Mises stress. Under greater swelling-induced softening, distortions induced by VF geometry change will likewise directly result in smaller stresses.

Swelling-induced mass, stiffness, and prephonatory gap changes were all found to increase viscous dissipation (Fig. 11) due to its dependence on tissue strain rates. Lowering stiffness, for example, tends to increase tissue deformations which would increase strain rates and thus increase viscous dissipation. Increasing mass tends to increase VF momentum which would also lead to higher viscous dissipation, particularly during contact, when the additional momentum is dissipated. Similarly, as swelling reduces the prephonatory gap, the VFs tend to collide with greater momentum, as evidenced by collision pressure (Tao et al. 2006; Titze 1994), which would lead to higher internal strain rate and greater viscous dissipation.

Effects of swelling-induced changes on collision pressure ($\hat{p}_c$) are explained by the momentum of the VFs at contact. The effect of swelling-induced softening on lowering collision pressure arises because the softer cover layer increases the time and area over which contact force is distributed. Swelling-induced mass variation tends to increase collision pressure (Fig. 11) likely due to the increase in momentum of the VFs, which was found to increase with increase in swelling. Similarly, swelling-induced prephonatory gap tends to cause increased collision pressure, as seen for smaller prephonatory gaps in past studies (Tao et al. 2006; Titze 1994), likely due to an increase in the pre-collision momentum.

All damage measures appear concentrated in the medial and superior portions of the cover (Figs. 5, 7, and 9). If von Mises stress ($\tilde{\sigma}_{vm}$) plays a dominant role in damage then swelling would be broadly distributed throughout the medial and superior portions of the cover (Fig. 5). In contrast, if collision pressure ($\tilde{p}_c$) and viscous dissipation ($\tilde{w}_{visc}$) drive damage, then swelling would likely concentrate at local regions on the medial surface, (Figs. 9 and 7).

Our results also suggest how swelling could play a role in initiating a vicious cycle that leads to PVH. The first aspect of the vicious cycle is a hyperfunctional response induced by changes in acoustic outputs from swelling. Our study shows that moderate amounts of swelling (30 %) induce relatively small changes in SPL (about 0.5 dB) and moderate changes in fundamental frequency (about 10 Hz) which suggests that hyperfunctional adjustments for voice changes induced by swelling would likely compensate for fundamental

frequency rather than loudness. Increases in fundamental frequency could be facilitated by compensatory hyperfunctional increases in muscle tension and subglottal pressure. Higher subglottal pressures would likely then trigger further swelling due to the damage induced by swelling as discussed previously. This could potentially lead to a vicious cycle and the development of PVH. We note that the simulations presented herein were performed at very low subglottal pressures, which was necessary to ensure self-sustained oscillations over the entire range of swelling parameters considered. We suspect that the impact of swelling on SPL and f_o would be more significant at higher subglottal pressures, but confirming this will require significant modifications to the methodology that are beyond the scope of this preliminary effort.

4.2 Study limitations

There are several important limitations in our study. First, three-dimensional (3D) effects are inherently omitted by virtue of the 2D model. Given the aspect ratio of fully adducted VFs, we expect that 3D simulation findings would be similar to the present results in a mid-coronal plane. That said, protuberances in the mid-membranous region evident in structural pathologies and their influence on VF dynamics cannot be accurately explored with a 2D model. Similarly, swelling localized to this region would require a full 3D simulation.

The third term in the first integral of Equation 1 represents viscous effects through a simple Kelvin–Voigt model, which is assumed herein to be unaffected by swelling. Hydration of the VFs is known to affect VF viscosity, with experiments finding that dehydration increases viscosity (Chan and Tayama 2002). This suggests that swelling, which increases water content, should lower viscosity. We expect that incorporating this effect will not significantly influence our results except for the viscous dissipation rate, since this measure is directly affected by viscous stresses. We hypothesize that modeling this effect will increase the viscous dissipation with swelling, $\tilde{w}_{visc}$, since the reduced viscosity will facilitate larger strain rates for the same external forcing. In addition, the Kelvin–Voigt model is a simple viscoelastic model that does not capture some viscoelastic behavior of VFs, such as shear thinning (Chan and Titze 1999, Figure 6). We opted to omit more complicated viscoelastic models and swelling effects on viscosity in order to focus our study on the change in shape and stiffness induced by swelling. More sophisticated viscoelastic models, like biphasic models, are more suited to investigate hydration-induced changes in viscosity and potentially capture viscoelastic phenomena like shear thinning. Coupling stress-driven fluid flux and swelling is left for future work.

Importantly, the present model does not incorporate physical mechanisms that cause swelling, such as chemical concentration

differences leading to osmotic pressure gradients. Our model considers swelling that is purely related to mechanical trauma; however, swelling is mediated and caused by numerous factors, such as presence of disease, changes in lymph drainage, and increases in capillary pressure (Mortimer and Levick 2004). While the current approach allows us to prescribe the level of swelling *a priori*, modeling the physical mechanisms that cause swelling is necessary for future studies examining the progression of phonotrauma. For example, in swelling induced by damage, the swelling profile would likely be concentrated near regions of local damage in contrast to the uniformly distributed swelling considered here. Consideration of physical mechanisms that cause swelling will be the subject of future work.

The subglottal pressure used in our model (300 Pa, Table 1) is lower than the typical value of about 1000 Pa used in many computational studies (see, for example, (Story and Titze 1995; Luo et al. 2008; Zheng et al. 2011)). In our simulations, we observed the hyperelastic material model predicted the VFs would adopt a static 'blown apart' configuration at subglottal pressures above about 500 Pa while the VFs would self-oscillate for intermediate pressures above the onset pressure but below this value. While this subglottal pressure is lower than the typical value employed in previous studies, it is within the lower end of the physiological range (Zhang 2016). Another study employing a different hyperelastic material model (Mooney–Rivlin) for the VFs (Movahhedi et al. 2021) coupled with a Bernoulli-based glottal flow used a subglottal pressure value of 2000 Pa but also modeled the VFs as three-dimensional and employed a different VF geometry. Extending the current model to three-dimensions along with modifications to VF geometry and constitutive models might allow for similarly high subglottal pressures to be employed while maintaining self-oscillation of the VFs. These higher subglottal pressures could also increase the effects of swelling on SPL and frequency seen here.

Our model does not include acoustic feedback effects (level 2 interactions (Titze 2008)) which could influence the VF dynamics with swelling. Given that the effects of swelling without acoustics induced relatively small changes, we suspect that acoustic coupling effects would likewise be minor. In special cases where the fundamental frequency is near a formant frequency, however, the changes in frequency induced by swelling could lead to dramatic changes in behavior due to resonance effects. Such acoustic feedback requires further investigation.

Finally, in the broader context of quantifying phonotrauma, there remains debate as to the most appropriate damage measure, with several having been proposed in the literature, including dissipation dose, contact pressures, and internal stresses (Titze 1994; Gunter 2004; Tao and Jiang 2007; Titze et al. 2003; Titze and Hunter 2015; Motie-Shirazi et al. 2021), which inspired the viscous dissipation metric employed herein (Titze et al. 2003; Motie-Shirazi et al. 2021). Furthermore, it remains

unclear whether localized damage or more distributed measures are most important and how these translate to swelling. The process leading from mechanical trauma to swelling involves a complex biochemical response at the cellular level which ultimately disturbs the normal fluid exchange through tissue Gou and Pence (2016). Whether localized or distributed measures of damage are more important then, would require detailed knowledge of how tissue damage affects these cellular mechanisms that control the fluid balance, which is incompletely understood Gou and Pence (2016). The measures explored herein were selected to canvas some of the parameters considered in prior literature for quantifying phonotrauma, but we make no claim that these are the best, nor even necessarily the most appropriate, measures to consider. As additional clinically validated measures are identified the influence of swelling should be reconsidered through their lens.

5 Conclusions

In this manuscript, we presented a first investigation into the impact of swelling distributed throughout the VF cover layer on VF kinematics and selected damage measures. At modest levels of swelling, the impacts were marginal, but grew as the degree of fluid accumulation increased. For example in terms of voice outputs, swelling consistently reduced fundamental frequency and SPL (a swelling value of 30 % induced around a 0.5 dB drop and 10 Hz drop in SPL and frequency, respectively). Such changes in voice outputs would lead to compensatory adjustments that could trigger the development of PVH.

Damage measures (von Mises stress, viscous dissipation, and collision pressure) were affected by swelling in different ways. In the case of von Mises stress, small values of swelling reduced average stresses in the cover due to a protective effect in the inferior portion of the cover while larger values of swelling increased von Mises stress depending on the amount of swelling-induced stiffness change (by about 40 % at swelling of $v = 1.3$ and swelling-induced softening of $\bar{m}' = -0.8$). Viscous dissipation consistently increased with increasing swelling and with greater swelling-induced stiffness change exacerbating the effect (by about 50 % at $v = 1.3$ and $\bar{m}' = -0.8$). Similarly, swelling tended to increase collision pressure (by about 75 % at $v = 1.3$ and $\bar{m}' = -0.8$) with increase in swelling, whereas greater swelling-induced stiffness change ameliorated the effect.

Swelling was decomposed into constituent effects to examine the factor that most contributed to observed trends in damage measures. Von Mises stress in the VFs was primarily affected by the swelling-induced shape and stiffness changes. In the inferior part of the cover, swelling-induced volume increases balanced with the compressive effects of the fluid loading resulting in decreases in von Mises stress.

In the medial and superior portions of the cover, however, the flow accelerates or separates resulting in little fluid loading and therefore von Mises stress increased under the effect of swelling. In contrast to the von Mises stress, viscous dissipation and collision pressures were affected primarily by swelling-induced mass, stiffness, and prephonatory gap, and not the VF geometry change (Fig. 11). In the case of swelling-induced stiffness, for example, we hypothesized the reduced stiffness tended to increase the magnitude of deformations which increased viscous dissipation; for collision pressure, the reduced stiffness would tend to distribute contact forces over longer times and areas, thus reducing average collision pressures.

Future work will aim to connect the distribution and magnitude of swelling with measures of damage. This will then be used to model the progressive effects of swelling with repeated voice usage due to the feedback of swelling-induced voice output changes leading to compensatory changes in the VFs that further increase swelling. To capture the important effects of swelling on viscoelastic parameters, coupling of swelling with biphasic models will also be pursued. Incorporating these two mechanisms will allow investigation of the etiology of PVH from phonotrauma.

Appendix A Swelling constitutive equation

Let the deformation from a reference configuration, X, to spatial coordinates, x, be given by $x = X + u(X)$. Then, $F = \partial u / \partial X$ is the deformation gradient and $E = 1/2(F^\top F - I)$ is the Green strain tensor. To incorporate the effects of swelling, Gou and Pence (Tsai et al. 2004; Pence and Tsai 2005a) proposed an extension of a hyperelastic strain energy ψ to the form (the strain energy is formulated here with dependence on E instead of F where the relation between the two strain energies is $\psi(E) = \psi(1/2(F^\top F - I)) = \psi(F)$)

$$\bar{\psi}(E;v) = m(v)\psi(\bar{E}(E;v)) \tag{A1}$$

where $\bar{\psi}$ is the swelling-generalized strain energy, ψ is the original strain energy, v is the swelling, and $m(v)$ is a scalar valued monotonic function that satisfies $m(1) = 1$. The swelling-modified deformation gradient is given by

$$\bar{F}(F;v) = v^{-1/3}F;$$

and the swelling-modified Green strain by

$$\bar{E}(E;v) = \frac{1}{2}(\bar{F}^T \bar{F} - I) = v^{-2/3}E + \frac{1}{2}(v^{-2/3} - 1)I.$$

The second Piola–Kirchhoff stress for the swelling-modified strain energy is

$$\begin{aligned}
\bar{S} &= \frac{\partial \bar{\psi}(E;v)}{\partial E} \\
&= m(v)\frac{\partial \psi(\bar{E})}{\partial \bar{E}}\frac{\partial \bar{E}}{\partial E} \\
&= m(v)v^{-2/3}\frac{\partial \psi(\bar{E})}{\partial \bar{E}} \\
&= m(v)v^{-2/3}S|_{\bar{E}(E;v)}
\end{aligned} \tag{A2}$$

For a Saint Venant–Kirchhoff material $\psi(E) = \lambda(\operatorname{Tr}E)^2 + \mu\operatorname{Tr}E^2$ so that the second Piola–Kirchhoff stress is

$$K_{ijkl} = \lambda\delta_{ij}\delta_{kl} + \mu(\delta_{ik}\delta_{jl} + \delta_{il}\delta_{jk}), \tag{A3}$$

$$S = KE = \lambda\operatorname{Tr}EI + 2\mu E, \tag{A4}$$

where μ and λ are Lame's parameters. Substituting the above [Eq. (A4)] into $\bar{S}$ [Eq. (A2)] results in

$$\bar{S} = \frac{m(v)}{v}v^{1/3}\left(\lambda\operatorname{Tr}\bar{E}I + 2\mu\bar{E},\right), \tag{A5}$$

where K is the constant elasticity tensor for a Saint Venant–Kirchhoff material.

To determine how $m(v)$ changes the modulus with swelling, consider the reference configuration coordinate, $X^\star$, corresponding to equiaxial expansion by the prescribed swelling such that $\partial X^\star / \partial X = v^{1/3}I$. The deformation gradient and Green strain measured with respect to the unswollen reference configuration, X, and with respect to the swollen reference configuration, $X^\star$, are then related by

$$F^\star = v^{-1/3}F$$

$$E^\star = \frac{1}{2}(F^{\star\top}F^\star - I) = v^{-2/3}E + \frac{1}{2}(v^{-2/3} - 1)I,$$

identical to the relation between $\bar{E}$ and E described above. The strain energy of the material with respect to the swollen reference configuration is

$$\psi^\star(E^\star;v) = m(v)\frac{\psi(\bar{E}(E,v))}{v} = m(v)\frac{\psi(E^\star)}{v}$$

where the factor $1/v$ is due to the volume increase. The tangent modulus with respect to the swollen configuration is then given by

$$\frac{\partial^2\psi^\star(E^\star;v)}{\partial(E^\star)^2} = \frac{m(v)}{v}\frac{\partial^2\psi(E^\star)}{\partial(E^\star)^2} = \frac{m(v)}{v}K,$$

where K is the elasticity tensor of the swollen material. This shows that the change in modulus is controlled by $m(v)/v$,

To simplify investigating different functional forms of $m(v)$, we approximate the effect of $m(v)/v$ with a linear approximation

$$\bar{S} \approx (\bar{m}'|_{v=1}(v-1)+1)v^{-1/3}\left(\lambda \operatorname{Tr} \bar{E}I + 2\mu\bar{E},\right) \quad (A6)$$

where $\bar{m} = m(v)/v$.

Appendix B Independence study

The mesh density in Fig. 1 and time step Δt were chosen based on a mesh and time step independence study shown in Fig. 12. The mean (over time and the cover region) for von Mises stress and viscous dissipation rate both converge to within 1 % of the finest discretization case (mesh size scale of 0.5 and Δt refinement factor of 16) by a Δt factor of 8 for the mesh refinement factor of 1. Errors in mean (over time) for contact force and area similarly converge by the same refinement condition. Therefore, a time step

of $\Delta t = 1.25 \times 10^{-5}$ s and the mesh refinement factor of 1 (corresponding to the mesh shown in Fig. 1) were chosen.

Data and materials availability Not applicable.

Declarations

Conflict of interest Matías Zañartu has a financial interest in Lanek SPA, a company focused on developing and commercializing biomedical devices and technologies. His interests were reviewed and are managed by the Universidad Técnica Federico Santa María in accordance with its conflict-of-interest policies.

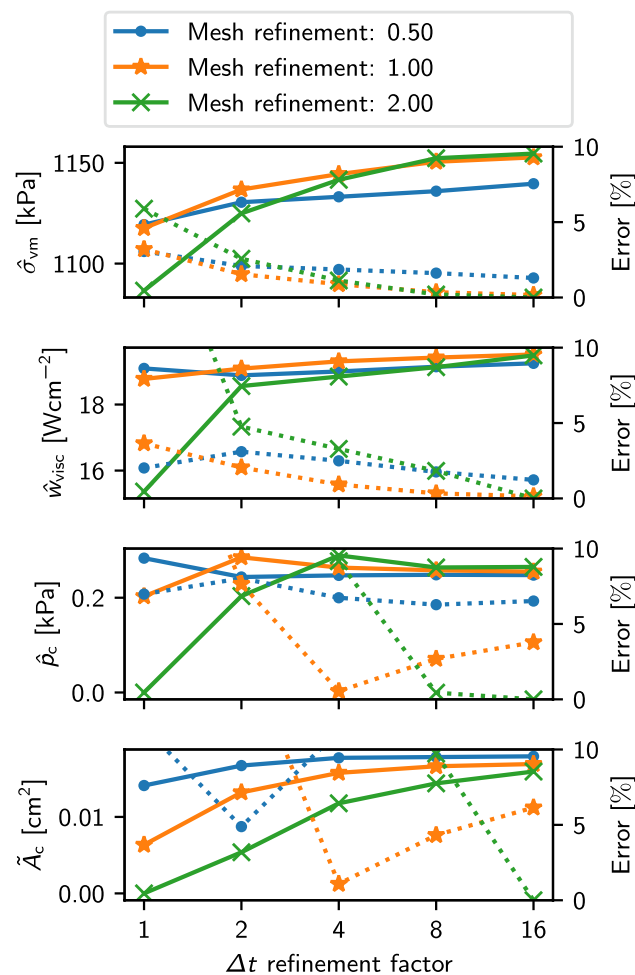**Ethical approval** Not applicable

Fig. 12 Mesh and time step independence study results in terms of four derived quantities for the case $(v, \bar{m}') = (1.3, -1.6)$. Solid lines show absolute values while dotted lines show errors relative to the finest mesh and time step case (mesh refinement of 2 and time step refinement of 16)

References

Alipour-Haghighi F, Berry DA, Titze IR (2000) A finite-element model of vocal-fold vibration. J Acoust Soc Am 108(6):3003–3012. https://doi.org/10.1121/1.1324678

Anderson P, Fels S, Green S (2013) Implementation and validation of a 1D fluid model for collapsible channels. J Biomech Eng 135(11):111006. https://doi.org/10.1115/1.4025326

Bastian RW, Keidar A, Verdolini-Marston K (1990) Simple vocal tasks for detecting vocal fold swelling. J Voice 4(2):172–183. https://doi.org/10.1016/S0892-1997(05)80144-4

Bathe KJ (2006) Finite element procedures, 2nd edn. Klaus-Jürgen Bathe, Watertown, MA

Bhattacharya P, Siegmund TH (2014) A computational study of systemic hydration in vocal fold collision. Comput Methods Biomech Biomed Engin 17(16):1835–1852. https://doi.org/10.1080/10255842.2013.772591

Chan RW, Tayama N (2002) Biomechanical effects of hydration in vocal fold tissues. Otolaryngol - Head Neck Surg 126(5):528–537. https://doi.org/10.1067/mhn.2002.124936

Chan RW, Titze IR (1999) Viscoelastic shear properties of human vocal fold mucosa: measurement methodology and empirical results. J Acoust Soc Am 106(4):2008–2021. https://doi.org/10.1121/1.427947

Chhetri DK, Zhang Z, Neubauer J (2011) Measurement of young's modulus of vocal folds by indentation. J Voice 25(1):1–7. https://doi.org/10.1016/j.jvoice.2009.09.005

Czerwonka L, Jiang JJ, Tao C (2008) Vocal nodules and edema may be due to vibration-induced rises in capillary pressure.

Laryngoscope 118(4):748–752. https://doi.org/10.1097/MLG.0b013e31815fdeee

Decker GZ, Thomson SL (2007) Computational simulations of vocal fold vibration: Bernoulli versus Navier-stokes. J Voice 21(3):273–284. https://doi.org/10.1016/j.jvoice.2005.12.002

Deng JJ, Peterson SD (2022) Examining the influence of epithelium layer modeling approaches on vocal fold kinematics and kinetics. Biomech Model Mechanobiol. https://doi.org/10.1007/s10237-022-01658-2

Elliot N, Sundberg J, Gramming P (1995) What happens during vocal warm-up? J Voice 9(1):37–44. https://doi.org/10.1016/S0892-1997(05)80221-8

Erath BD, Zañartu M, Peterson SD (2017) Modeling viscous dissipation during vocal fold contact: the influence of tissue viscosity and thickness with implications for hydration. Biomech Model Mechanobiol 16(3):947–960. https://doi.org/10.1007/s10237-016-0863-5

Friedman JN, Goldman RD, Srivastava R et al (2004) Development of a clinical dehydration scale for use in children between 1 and 36 months of age. J Pediatr 145(2):201–207. https://doi.org/10.1016/j.jpeds.2004.05.035

Fung YC (1993) Biomechanics, 2nd edn. Springer, New York, NY. https://doi.org/10.1007/978-1-4757-2257-4

Gou K, Pence TJ (2016) Hyperelastic modeling of swelling in fibrous soft tissue with application to tracheal angioedema. J Math Biol 72(1–2):499–526. https://doi.org/10.1007/s00285-015-0893-0

Gou K, Topol H, Demirkoparan H et al (2020) Stress-swelling finite element modeling of cervical response with homeostatic collagen fiber distributions. J Biomech Eng 142(8):80–90. https://doi.org/10.1115/1.4045810

Gunter HE (2004) Modeling mechanical stresses as a factor in the etiology of benign vocal fold lesions. J Biomech 37(7):1119–1124. https://doi.org/10.1016/j.jbiomech.2003.11.007

Gurtin ME, Fried E, Anand L (2010) The mechanics and thermodynamics of continua. Cambridge University Press, Cambridge. https://doi.org/10.1017/CBO9780511762956

Hadwin PJ, Motie-Shirazi M, Erath BD et al (2019) Bayesian inference of vocal fold material properties from glottal area waveforms using a 2D finite element model. Appl Sci 9(13):2735. https://doi.org/10.3390/app9132735

Hadwin PJ, Erath BD, Peterson SD (2021) The influence of flow model selection on finite element model parameter estimation using Bayesian inference. JASA Express Lett 1(4):045,204. https://doi.org/10.1121/10.0004260

Hansbo P, Larson MG (2014) Finite element modeling of a linear membrane shell problem using tangential differential calculus. Comput Methods Appl Mech Eng 270:1–14. https://doi.org/10.1016/j.cma.2013.11.016

Hillman RE, Stepp CE, Van Stan JH et al (2020) An updated theoretical framework for vocal hyperfunction. Am J Speech-Language Pathol 29(4):2254–2260. https://doi.org/10.1044/2020_AJSLP-20-00104

Hirano M (1974) Morphological Structure of the Vocal Cord as a Vibrator and its Variations. Folia Phoniatr Logop 26(2):89–94. https://doi.org/10.1159/000263771

Hirano M, Kakita Y (1985) Cover-body theory of vocal fold vibration. In: Daniloff R (ed) Speech Sci. College-Hill Press, San Diego, CA, Recent Adv, pp 1–46

Holmberg EB, Hillman RE, Perkell JS et al (1994) Relationships between intra-speaker variation in aerodynamic measures of voice production and variation in SPL across repeated recordings. J Speech Hear Res 37(3):484–495. https://doi.org/10.1044/jshr.3703.484

King RE, Steed K, Rivera AE et al (2018) Magnetic resonance imaging quantification of dehydration and rehydration in vocal fold tissue

layers. PLoS One 13(12):1–17. https://doi.org/10.1371/journal.pone.0208763

Kinsler LE, Frey AR, Coppens AB et al (2000) Fundamentals of acoustics, 4th edn. John Wiley and Sons, Hoboken

Lai WM, Hou JS, Mow VC (1991) A triphasic theory for the swelling and deformation behaviors of articular cartilage. J Biomech Eng 113(3):245–258. https://doi.org/10.1115/1.2894880

Logg A, Wells GN (2010) DOLFIN. ACM Trans Math Softw 37(2):1–28. https://doi.org/10.1145/1731022.1731030

Logg A, Kent-Andre M, Wells GN (2012) Automated solution of differential equations by the finite element method, lecture notes in computational science and engineering. Springer, Berlin, Heidelberg. https://doi.org/10.1007/978-3-642-23099-8

Luo H, Mittal R, Zheng X et al (2008) An immersed-boundary method for flow-structure interaction in biological systems with application to phonation. J Comput Phys 227(22):9303–9332. https://doi.org/10.1016/j.jcp.2008.05.001

Milbrath RL, Solomon NP (2003) Do vocal warm-up exercises alleviate vocal fatigue? J Speech, Lang Hear Res 46(2):422–436. https://doi.org/10.1044/1092-4388(2003/035)

Miri AK (2014) Mechanical characterization of vocal fold tissue: a review study. J Voice 28(6):657–667. https://doi.org/10.1016/j.jvoice.2014.03.001

Mortimer PS, Levick JR (2004) Chronic peripheral oedema: the critical role of the lymphatic system. Clin Med J R Coll Physicians London 4(5):448–453. https://doi.org/10.7861/clinmedicine.4-5-448

Motie-Shirazi M, Zañartu M, Peterson SD et al (2021) Vocal fold dynamics in a synthetic self-oscillating model: contact pressure and dissipated-energy dose. J Acoust Soc Am 150(1):478–489. https://doi.org/10.1121/10.0005596

Movahhedi M, Geng B, Xue Q et al (2021) Effects of cricothyroid and thyroarytenoid interaction on voice control: muscle activity, vocal fold biomechanics, flow, and acoustics. J Acoust Soc Am 150(1):29–42. https://doi.org/10.1121/10.0005275

Murray PR, Thomson SL (2012) Vibratory responses of synthetic, self-oscillating vocal fold models. J Acoust Soc Am 132(5):3428–3438. https://doi.org/10.1121/1.4754551

Newmark NM (1962) A method of computation for structural dynamics. Trans Am Soc Civ Eng 127(1):1406–1433. https://doi.org/10.1061/TACEAT.0008448

Oates J, Winkworth A (2008) Current knowledge, controversies and future directions in hyperfunctional voice disorders. Int J Speech Lang Pathol 10(4):267–277. https://doi.org/10.1080/17549500802140153

Pence TJ, Tsai H (2005) On the cavitation of a swollen compressible sphere in finite elasticity. Int J Non Linear Mech 40(2–3):307–321. https://doi.org/10.1016/j.ijnonlinmec.2004.06.004

Pence TJ, Tsai H (2005) Swelling-induced microchannel formation in nonlinear elasticity. IMA J Appl Math Institute Math Its Appl 70(1):173–189. https://doi.org/10.1093/imamat/hxh049

Scherer RC, Shinwari D, De Witt KJ et al (2001) Intraglottal pressure profiles for a symmetric and oblique glottis with a divergence angle of 10 degrees. J Acoust Soc Am 109(4):1616–1630. https://doi.org/10.1121/1.1333420

Starling EH (1896) On the absorption of fluids from the connective tissue spaces. J Physiol 19(4):312–326. https://doi.org/10.1113/jphysiol.1896.sp000596

Story BH, Titze IR (1995) Voice simulation with a body-cover model of the vocal folds. J Acoust Soc Am 97(2):1249–1260. https://doi.org/10.1121/1.412234

Tao C, Jiang JJ (2007) Mechanical stress during phonation in a self-oscillating finite-element vocal fold model. J Biomech 40(10):2191–2198. https://doi.org/10.1016/j.jbiomech.2006.10.030

Tao C, Jiang JJ, Zhang Y (2006) Simulation of vocal fold impact pressures with a self-oscillating finite-element model. J Acoust Soc Am 119(6):3987–3994. https://doi.org/10.1121/1.2197798

Titze IR (1994) Mechanical stress in phonation. J Voice 8(2):99–105. https://doi.org/10.1016/S0892-1997(05)80302-9

Titze IR (2008) Nonlinear source-filter coupling in phonation: theory. J Acoust Soc Am 123(5):2733–2749. https://doi.org/10.1121/1.2832337

Titze IR, Hunter EJ (2015) Comparison of vocal vibration-dose measures for potential-damage risk criteria. J Speech, Lang Hear Res 58(5):1425–1439. https://doi.org/10.1044/2015_JSLHR-S-13-0128

Titze IR, Švec JG, Popolo PS (2003) Vocal dose measures. J Speech, Lang Hear Res 46(4):919–932. https://doi.org/10.1044/1092-4388(2003/072)

Topol H, Gou K, Demirkoparan H et al (2018) Hyperelastic modeling of the combined effects of tissue swelling and deformation-related collagen renewal in fibrous soft tissue. Biomech Model Mechanobiol 17(6):1543–1567. https://doi.org/10.1007/s10237-018-1043-6

Tsai H, Pence TJ, Kirkinis E (2004) Swelling induced finite strain flexure in a rectangular block of an isotropic elastic material. J Elast 75(1):69–89. https://doi.org/10.1023/B:ELAS.0000039924.09593.72

Tse JR, Zhang Z, Long JL (2015) Effects of vocal fold epithelium removal on vibration in an excised human larynx model. J Acoust Soc Am 138(1):EL60–EL64. https://doi.org/10.1121/1.4922765

Verdolini K, Rosen CA, Branski RC et al (2003) Shifts in biochemical markers associated with wound healing in laryngeal secretions following phonotrauma: a preliminary study. Ann Otol Rhinol Laryngol 112(12):1021–1025. https://doi.org/10.1177/000348940311201205

Vintturi J, Alku P, Lauri ER et al (2001) Objective analysis of vocal warm-up with special reference to ergonomic factors. J Voice 15(1):36–53. https://doi.org/10.1016/S0892-1997(01)00005-4

Wilson W, Van Donkelaar CC, Huyghe JM (2005) A comparison between mechano-electrochemical and biphasic swelling theories for soft hydrated tissues. J Biomech Eng 127(1):158–165. https://doi.org/10.1115/1.1835361

Wriggers P (2006) Computational contact mechanics, 2nd edn. Springer, Berlin, Heidelberg. https://doi.org/10.1007/978-3-540-32609-0

Wu L, Zhang Z (2017) A computational study of vocal fold dehydration during phonation. IEEE Trans Biomed Eng 64(12):2938–2948. https://doi.org/10.1109/TBME.2017.2691399

Wu L, Zhang Z (2022) Computational study of the impact of dehydration-induced vocal fold stiffness changes on voice production. J Voice. https://doi.org/10.1016/j.jvoice.2022.02.001

Xuan Y, Zhang Z (2014) Influence of embedded fibers and an epithelium layer on the glottal closure pattern in a physical vocal fold model. J Speech, Lang Hear Res 57(2):416–425. https://doi.org/10.1044/2013_JSLHR-S-13-0068

Yang J, Wang X, Krane M et al (2017) Fully-coupled aeroelastic simulation with fluid compressibility - For application to vocal fold vibration. Comput Methods Appl Mech Eng 315:584–606. https://doi.org/10.1016/j.cma.2016.11.010

Yang S, Zhang Y, Mills RD et al (2017) Quantitative study of the effects of dehydration on the viscoelastic parameters in the vocal fold mucosa. J Voice 31(3):269–274. https://doi.org/10.1016/j.jvoice.2016.05.002

Zhang Y, Czerwonka L, Tao C et al (2008) A biphasic theory for the viscoelastic behaviors of vocal fold lamina propria in stress relaxation. J Acoust Soc Am 123(3):1627–1636. https://doi.org/10.1121/1.2831739

Zhang Z (2016) Respiratory laryngeal coordination in airflow conservation and reduction of respiratory effort of phonation. J Voice 30(6):760.e7–760.e13. https://doi.org/10.1016/j.jvoice.2015.09.015

Zheng X, Xue Q, Mittal R et al (2010) A coupled sharp-interface immersed boundary-finite-element method for flow-structure interaction with application to human phonation. J Biomech Eng 132(11):111,003. https://doi.org/10.1115/1.4002587

Zheng X, Mittal R, Xue Q et al (2011) Direct-numerical simulation of the glottal jet and vocal-fold dynamics in a three-dimensional laryngeal model. J Acoust Soc Am 130(1):404–415. https://doi.org/10.1121/1.3592216